Proceedings of the INMM & ESARDA – Joint Annual Meeting
May 22-26, 2023

Investigation on Structural Incorporation of Dopants into Uranium Oxide Structure Considering the Development of New Composite Reference Microparticles

Shannon Kimberly Potts[1], Philip Kegler[1], Giuseppe Modolo[1], Simon Hammerich[2], Martina Klinkenberg[1], Irmgard Niemeyer[1], Dirk Bosbach[1], Stefan Neumeier[1]

[1] Forschungszentrum Jülich GmbH, Institute of Energy and Climate Research – Nuclear Waste Management (IEK-6), 52428 Jülich, Germany

[2] Heidelberg University, Institute of Earth Sciences, 69120 Heidelberg, Germany

Corresponding author: Shannon Kimberly Potts; E-mail: s.potts@fz-juelich.de

ABSTRACT

In the Safeguards laboratories of Forschungszentrum Juelich an aerosol-based process to produce uranium oxide reference microparticles has been implemented to support a sustainably robust quality control system of the International Atomic Energy Agency (IAEA) in particle analysis in nuclear safeguards. This quality control system includes analytical instrument calibration, method development and validation for analytical measurements of individual micrometer- and
Submicrometer-sized particles as well as their application in interlaboratory exercises. The well-designed reference microparticles developed for this purpose must fulfil certain requirements, such as a defined elemental and isotopic composition, size, morphology, and shelf-life, to ensure the reliability of the mass spectrometric analytical measurements and to be as similar as possible to the U-containing microparticles collected by an IAEA safeguards inspector during in-field verification activities. These so-called environmental samples are analyzed for their isotopic composition by the IAEA's Office of Safeguards Analytical Services and their dedicated Network of Analytical Laboratories. For the detection of even traces of fission products further development of analytical methods and the quality control of the analytical results from particle analysis itself as well as of the reference microparticles is required. But due to the yield limitations to microgram range of the aerosol-based process in Juelich, the characterization of these simulated fission products doped uranium-oxide microparticles is very challenging. Therefore, to unravel the incorporation mechanism of the dopants, such as lanthanides, Th, or Pu, into the uranium-oxide structure, a co-precipitation method was adjusted to produce doped bulk-scale materials as "internal refence materials" which can be investigated by standard analytical techniques. Using TG-DSC measurements, the temperature range of the phase transition from UO_3 to U_3O_8 of the doped uranium-containing materials was determined. According to the previously identified temperature ranges, the doped materials were calcined and the obtained doped UO_3 and U_3O_8 materials were characterized in more detail by additional systematic structural investigations of the long- and short-range order phenomena with XRD and Raman. This presentation will show results regarding the incorporation of dopants into the uranium oxide structures. These results will be transferred to the particle production process as an important input parameter to design reference microparticles.

INTRODUCTION

In order to verify the compliance with the Treaty of Non-Proliferation (NPT) of the member states, the IAEA sends inspectors to nuclear facilities. During the inspection the inspector *inter alia,* takes swipe samples, which contain U-bearing microparticles. These microparticles are analyzed by mass spectrometric analytic methods such as Large Geometry-Secondary Ion Mass Spectrometry (LG-SIMS) in their isotopic compositions, especially the isotope ratios $n(^{236}U)/n(^{238}U)$ and $n(^{235}U)/n(^{238}U)$, which evaluate the absence of undeclared nuclear materials and activities [1], [2]. To ensure Quality Assurance and Control (QA/QC) of analytical measurements on nuclear safeguards samples and to maintain the credibility of the IAEA with its Member States, the IAEA expressed a significant demand on uranium-based reference materials. Due to this request, a physical aerosol-based approach was implemented in the safeguards laboratories at Forschungszentrum Jülich leading to the production of certified microparticulate uranium-oxide reference materials [3]-[6] with precisely defined elemental and isotopic composition, size, morphology, and with a certain shelf-life [7].
To increase the selectivity and the sensitivity of the mass spectrometric analysis method in order to be able to detect small amounts of fission products and other isotope ratios such as $n(^{230}Th)/n(^{234}U)$, which is of interest for age-dating of U-bearing materials in general and for the IAEA in particular, the uranium oxide reference materials have to be further developed in the direction of composite (U-lanthanides (*Ln*'s), U-Th and U-Pu) reference materials in microparticulate form [7], [8]. To be able to produce such composite microparticles and to draw conclusions about the stability and shelf-life of the particles, the incorporation behaviour of the dopants in the uranium-oxide structure must be investigated. However, this is an analytical challenge, particularly in view of investigations on the structural incorporation of the dopants and consecutively on the stability of the materials since the quantities of material that are produced with the physical aerosol-based set-up in Juelich are limited. Therefore, a synthesis route was adapted to produce ammonium diuranate (ADU) doped with various *Ln*'s [9], [10] and Th as a sort of "internal reference materials" which serve as a bulky model system for comparison. These "internal reference materials" were calcined at defined temperatures and characterized in order to investigate the structural incorporation of the dopants into the uranium-oxide structure and to transfer these findings to the microparticulate system [8], [9]. This proceedings paper discusses the investigation of 1 mol% Th-doped uranium materials.

EXPERIMENTAL

The synthesis of 1 mol% Th-doped ADU ($(NH_4)_2U_2O_7$) was adapted from Kegler *et al.* [11]. An aqueous uranyl nitrate ($UO_2(NO_3)_2 \cdot 6\ H_2O$) solution and an aqueous solution of thorium nitrate ($Th(NO_3)_4$) were mixed together and the mixed solutions were slowly added to conc. NH_3 while stirring. After two hours of stirring the synthesized material was washed several times with MilliQ® water and finally elutriated with ethanol and dried.
Thermogravimetric analyses and differential scanning calorimetry (TG-DSC) measurements via a NETZSCH STA 449 F1 Jupiter was used to identify the thermally induced phase formation of the 1 mol% Th-doped ADU. For the measurement, Pt/Rh crucible was used with a heating rate of 10 $K \cdot min^{-1}$ in synthetic air (80/20). Afterwards the sample was calcined at 520 °C and 700 °C for 5 h. In order to investigate the chemical composition of the calcined 1 mol% Th-doped samples, X-ray Diffraction (XRD) measurements were performed by using a Bruker D4 Endeavor diffractometer equipped with a 1*D* Lynx-eye detector in Bragg-Brentano configuration using Cu $K_{\alpha 1,2}$ radiation (λ =1.54184 Å). XRD data were collected at room

temperature in the $10° \leq 2\theta \leq 120°$ range with a step size of $(2\theta) = 0.01°$ and a counting time of 2 s per step, leading to a total counting time of about 6 hours. Lattice parameters were refined by the Rietveld method using GSAS2 software [12]. To measure the short-range order phenomena, Raman measurements of the calcined 1 mol% Th-doped samples were performed at room temperature in the range of 100 cm^{-1} to 1000 cm^{-1} with a spectral resolution of around 1 cm^{-1} and a slit of 100 µm using a Horiba LabRAM HR spectrometer with a Peltier-cooled multichannel CCD detector with a He–Ne laser at a power of 17 mW (λ = 632.8 nm). For the measurements, small quantities of the calcined powders had to be glued onto carbon adhesive tabs.

RESULTS

The 1 mol% Th-doped ADU sample, produced via co-precipitation, were investigated to understand the incorporation mechanism of the Th into the uranium oxide structure using state-of-the-art analytical methods. To analyze the decomposition of the Th-doped ADU as well as to identify the temperature ranges where phase transitions occur, a TG-DSC measurement (Figure 1) was performed and compared to the decomposition behavior of the undoped ADU published by Potts *et al*. [10]. Figure 1 shows the mass loss as well as the DSC signal of the 1 mol% Th-doped ADU as a function of the calcination temperature. The observed mass loss and the endothermic DSC signal up to a temperature of 283 °C correspond to the removal of H_2O and the subsequent two exothermic DSC signals at 307 °C and 405 °C most likely to the NH_3 release according to the literature [13]. The initial decomposition of the doped material is very similar to the decomposition behavior of the undoped material [10]. The shoulder of the exothermic DSC signal at around 428 °C indicates that a second exothermal transition takes place. Since no significant mass loss of the TG signal is linked to the exothermal transition, it can be assigned to the formation of β-UO_3 phase which, according to the literature [10], [13], can be formed in this temperature region. The significant mass loss in the temperature range from 520 °C to 635 °C can be assigned to the formation of U_3O_8. The broad mass loss step indicates that the phase transition to U_3O_8 is not a monophasic transition. This indication is supported by the endothermic DSC signal with a pronounced plateau, indicating a gradual decomposition as it is known for the decomposition of amorphous phase and is also observed for the undoped ADU [10]. The amorphous phase is described in the literature as either stoichiometric U_2O_7 [14], [15] or an amorphous UO_3 hydrate [16], which during the phase transition gradually converts to the intermediate α-$UO_{2.9}$ and then to U_3O_8 [17]. The absence of an exothermic DSC signal, which indicates the crystallization of the amorphous phase could be overlapped by a competing phase transitions and also explains the lower reaction enthalpy of the phase transformation to U_3O_8 for the 1 mol% Th-doped sample (38.(2) $kJ \cdot mol^{-1}$) compared to the undoped sample (55.(5) $kJ \cdot mol^{-1}$) [10]. After the phase transformation, the material is present as U_3O_8. However, it can also be observed that by doping the material, the region of the phase transformation to U_3O_8 is shifted to a lower temperature range, which can be seen by comparing the temperatures of the maxima of the endothermic DSC signal T_p of the transition (undoped: $T_{p,1}$ = 583.5°C, $T_{p,2}$ = 609.7 °C; Th-doped: $T_{p,1}$ = 574.2°C, $T_{p,2}$ = 582.7 °C). These observations indicate that doping with 1 mol% Th affects the phase transformation from UO_3 to U_3O_8.

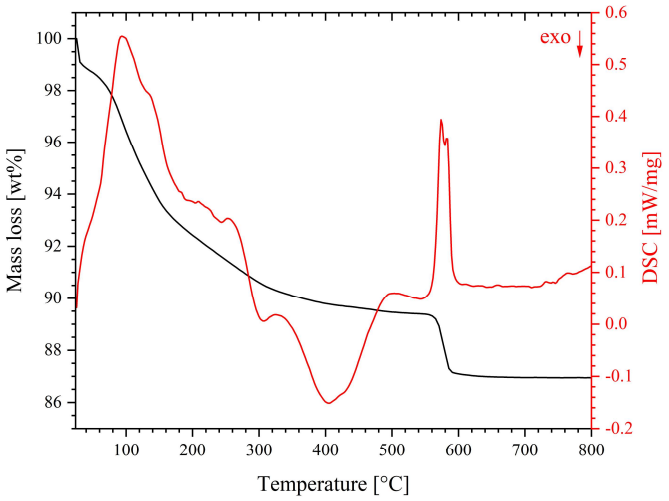

Figure 1: TG-DSC data obtained during heating of 1 mol% Th-doped $(NH_4)_2U_2O_7$ from room temperature to 800 °C measured in synthetic air.

To investigate the phase transformation to U_3O_8, the 1 mol% Th-doped ADU was subsequently calcined at 520 °C and 700 °C. The chosen calcination temperatures were derived from the TG-DSC thermogram. In order to evaluate the composition after calcination at 520 °C and 700 °C, the 1 mol% Th-doped samples were structurally investigated using XRD and Raman.

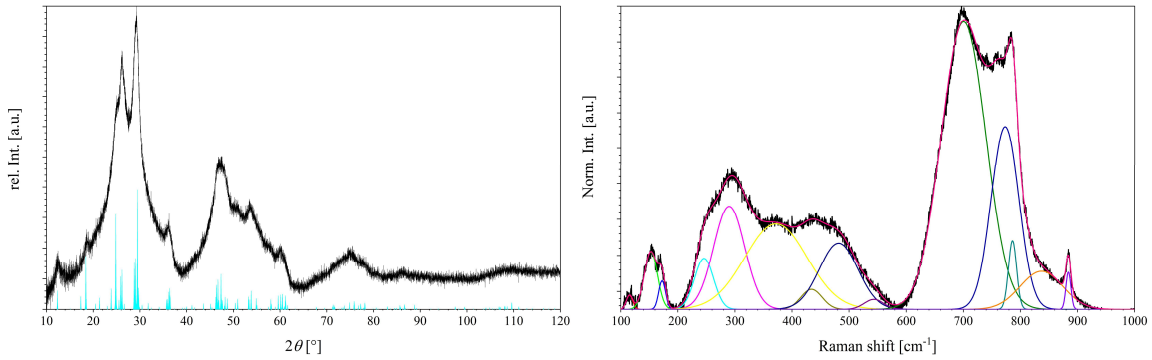

Figure 2: X-ray diffractogram (left) and Raman (right) spectrum of the 1 mol% Th-doped sample after calcination at 520 °C (Reference: α-UO_3 with the space group *P2₁* (cyan) [18]).

Figure 2 shows the structural investigations of the 1 mol% Th-doped sample after calcination at 520 °C. The XRD measurement of the calcined Th-doped material (Figure 2 left) indicate the formation of a phase mixture of α-UO_3 and an amorphous phase, which shows significantly higher proportions of an amorphous phase compared to the calcined undoped ADU published by Potts *et al.* [10]. The broad reflexes of the 1 mol% Th-doped sample after calcination at 520 °C indicate a preferred formation of β-UO_3 and shows a different formation behavior than the undoped calcined ADU, which show the formation of α-UO_3 and β-UO_3 phases. The increased amorphous fraction of the 1 mol% Th-doped sample indicates that the Th stabilized the amorphous phase. This assumption is supported by broadening and less observed vibrational modes in the Raman (Figure 2 right) spectrum of the Th-doped sample compared to the calcined undoped sample [10]. The observed vibrational modes of the Th-doped material (Table 1) only indicate the formation of UO_3 [19]-[22] and show no significant vibrations of ThO_2 [23].

Table 1: Measured Raman band positions, relative intensities normalized to maximum and observed band width in comparison to literature values of the 1 mol% Th-doped sample after calcination at 520 °C.

Raman	Center [cm^{-1}]	Phase	Band Assignment	Ref.
115 ± 1 (w)	116 (w)	β-UO_3	-	[19]
153 ± 1 (m)	158-159 (w-m)	β-UO_3	-	[19]
172 ± 1 (m)	174 (m)	β-UO_3	-	[19]
	171 (w-m)	α-UO_3	Symmetric δ of O-U-O	[20]
246 ± 2 (m)	~ 265 (w-m)	β-UO_3	-	[19], [21]
	253 (w-m)	α-UO_3		[22]
290 ± 2 (m-s)	283-305 (w-m)	β-UO_3	-	[19]
372 ± 7 (m, br)	377-406 (w-m, br)	β-UO_3	-	[19]
	393 (w)	α-UO_3		[22]
434 ± 7 (w)	~ 445 (m-s)	β-UO_3	-	[19], [21]
	446 (w)	α-UO_3	-	[20]
482 ± 10 (m)	~ 478 (w-s)	β-UO_3	-	[19], [21]
	476 (w)	α-UO_3	-	[20]
544 ± 8 (w)	495 (w)	α-UO_3, β-UO_3	-	[19], [22]
570 ± 2 (m-s)	575 (w)	α-UO_3	-	[22]
700 ± 1 (s)	699 (m-s)	β-UO_3	U-O symmetric stretching	[19]
773 ± 1 (m-s)	770 (m)	β-UO_3	UO_2^{2+} symmetric stretching	[19]
	760 (m)	α-UO_3	U-O stretching	[20]
786 ± 1 (s)	788(s)	β-UO_3	UO_2^{2+} symmetric stretching	[19]
837 ± 6 (w)	851 (w)	β-UO_3	UO_2^{2+} symmetric stretching	[19]
	836-850 (s)	α-UO_3	Pseudo UO_2^{2+} symmetric stretching	[20], [22]
884 ± 1 (w-m)	886 (m-s)	β-UO_3	UO_2^{2+} symmetric stretching	[19]

(s = strong, m = medium, w = weak, br = broad)

As a comparison, a pure Th sample was synthesized using $Th(NO_3)_4$ and NH_3 by the co-precipitation method and then calcined at 520 °C for 5 h. The XRD (Figure 3) shows the formation of crystalline cubic ThO_2 under the given synthesis conditions and indicates that due to the missing ThO_2 reflections in the diffractogram as well as missing characteristic ThO_2 bands in the Raman spectrum of the 1 mol% Th-doped sample, the Th as a dopant is somehow incorporated into the uranium oxide structure.

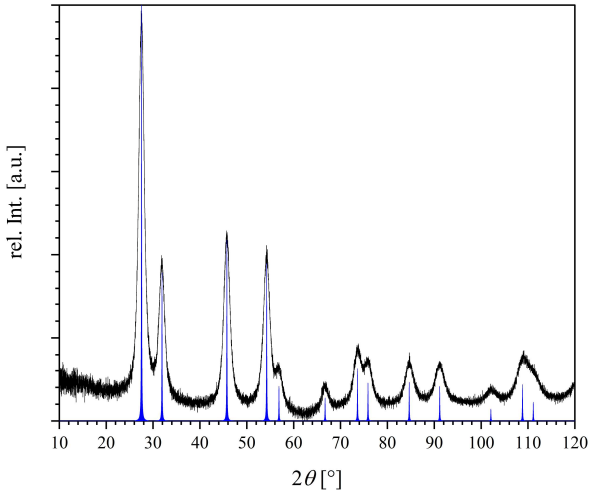

Figure 3: X-ray diffractogram of a pure Th sample after calcination at 520 °C (Reference: ThO_2 with a space group $Fm\bar{3}m$ (blue) [24]).

In order to investigate the material after the phase transformation to U_3O_8, the 1 mol% Th-doped ADU was calcined at 700 °C and investigated with XRD and Raman spectroscopy. In

Figure 4, the measured X-ray diffractogram and Raman spectrum are shown. The XRD pattern of the calcined 1 mol% Th-doped sample (Figure 4 left) shows the formation of an orthorhombic α-U_3O_8 phase with the space group *C2mm* [25] comparable to the undoped ADU after calcination at 700 °C published by Potts *et al*. [9]. However, the XRD pattern of the doped sample shows a convergence of the double reflexes at about 2θ values of 26° and 34° (Figure 5, left (zoom in)). This indicates that the lattice parameters and consequently the volume of the unit cell changed and indicates Th is incorporated into the U_3O_8 structure. The lattice of the 1 mol% Th-doped sample determined via Rietveld refinement is 333.41(3) $Å^3$ and shows a lattice volume expansion of 0.33(2) $Å^3$ compared to the pure U_3O_8 (333.08(1) $Å^3$)[10]. Since the Th^{4+}-ion has a larger ionic radius ($r(Th^{4+})$ = 1.08 Å) [26] than the uranium ions in the U_3O_8 structure ($r(U^{6+})$ = 0.87 Å; $r(U^{5+})$ = 0.9 Å) [26], the volume expansion indicates the Th-substitution at the uranium site. Something similar was observed by Asplanato *et al.* [27]. But according to phase diagram of Paul *et al.* [28], either a U_3O_8 and M_4O_9 or a U_3O_8 and MO_{2+x} phase mixture should result.

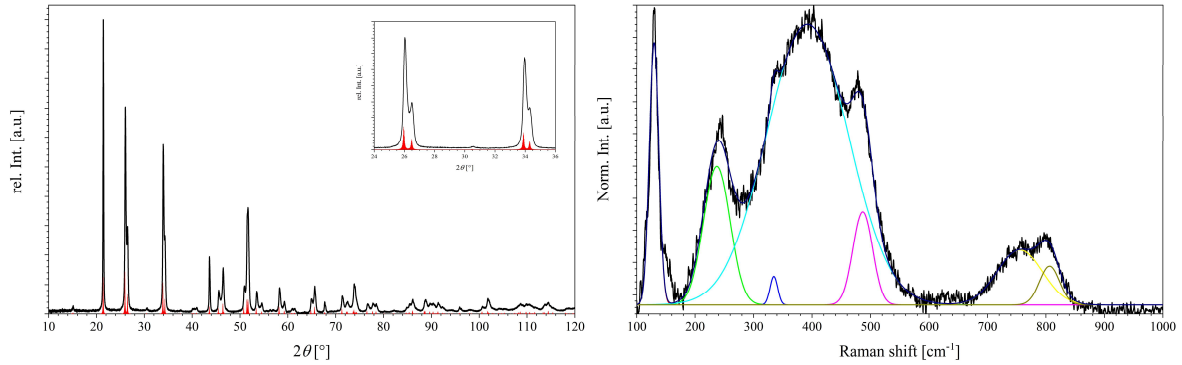

Figure 4: X-ray diffractogram (left) and Raman (right) spectrum of the 1 mol% Th -doped sample after calcination at 700 °C (Reference: α-U_3O_8 with the space group *C2mm* (red) [25]).

Therefore, Raman and IR measurements were performed with the 1 mol% Th-doped sample to verify the absence of additional segregated Th-rich phases, such as M_4O_9 or MO_{2+x} phases in the short-range order. The measured Raman and IR spectra (Figure 4 b and 4 c, Table 2) of the Th-doped material only indicate the formation of U_3O_8 and show no significant vibrations of ThO_2 (Raman: 465 cm^{-1}) [23] or doped UO_2 (Raman: 445 cm^{-1}) [29] and U_4O_9 (Raman: 450 cm^{-1} and broad band between 500 cm^{-1} and 700 cm^{-1}) [29]-[31]. In order to obtain a better comparability to the observations of Paul *et al.* [28] and Asplanato *et al.* [27], the 1 mol% Th-doped sample was calcined at a temperature of 1200 °C. Figure 5 shows the obtained X-ray diffractogram of the Th-doped sample after the calcination.

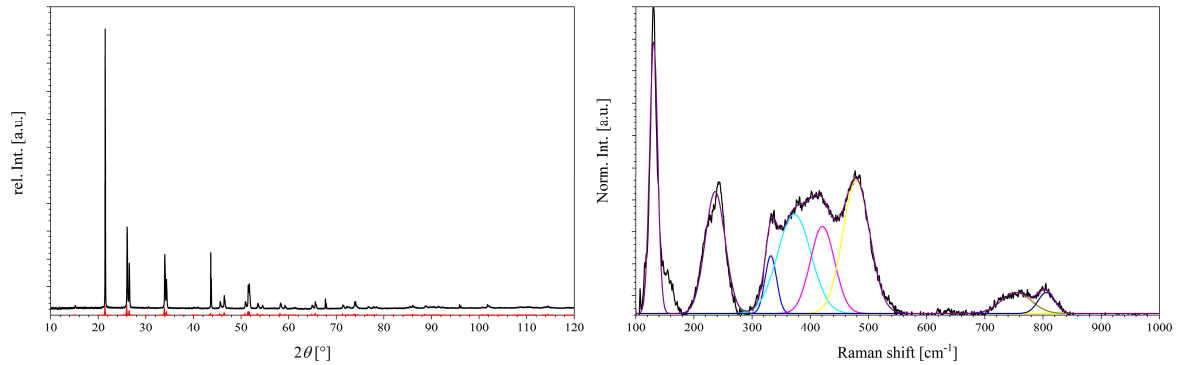

Figure 5: X-ray diffractogram (left) and Raman (right) spectrum of the 1 mol% Th-doped sample after calcination at 1200 °C (Reference: α-U_3O_8 with the space group *C2mm* (red) [25]).

Table 2: Measured Raman band positions, relative intensities normalized to maximum and observed band width in comparison to literature values of the 1 mol% Th-doped sample after calcination at 700 °C and 1200 °C.

After calcination at 700 °C	After calcination at 1200 °C	Center [cm^{-1}]	Phase	Band Assignment	Ref.
130 ± 1 (s)	131 ± 1 (s)	130 (w-s)	U_3O_8	Line of uncertain origin	[32], [33]
237 ± 1 (m-s)	236 ± 1 (m-s)	230-243 (w-s)	U_3O_8	Line of uncertain origin	[32]-[45]
335 ± 1 (w-m)	332 ± 1 (m-s)	335-51 (m)	U_3O_8	U-O stretching	[32]-[45]
-	372 ± 3 (m)	372 (w-m)	U_3O_8	-	[45]
392 ± 1 (s, br)	421 ± 2 (m-s)	405-421 (s)	U_3O_8	U-O stretching	[32]-[45]
487 ± 1 (m)	478 ± 1 (m-s)	474-488 (m)	U_3O_8	U-O stretching	[32]-[45]
755 ± 3 (w-m, br)	754 ± 3 (w-m, br)	731-753 (w-m)	U_3O_8	O-U-O stretching	[32]-[45]
806 ± 1 (w)	806 ± 2 (w)	798-820 (w-m)	U_3O_8	U-O stretching	[32]-[45]

(s = strong, m = medium, w = weak, br = broad)

The diffractogram shows, similar to the sample calcined at 700 °C, the formation of orthorhombic U_3O_8 with a space group of *C2mm*. The Raman spectrum shows only the U_3O_8 vibrations (Figure 5 left, Table 2). This indicates that the Th is still incorporated into the U_3O_8 structure and no formation of M_4O_9, MO_{2+x} or ThO_2 phases could be observed similar to the observations of Asplanato *et al.* [27]. This leads to the same conclusion as in the publication of Asplanato *et al.* [27] that Th with 1 mol% as doping content can be incorporated into the orthorhombic U_3O_8 structure.

CONCLUSION

The structural reaction of the formed uranium oxide phases before and after the phase transformation to U_3O_8 was investigated in the presence of Th as a dopant. It could be shown that already 1 mol% Th influences the phase transformation to U_3O_8. In addition, it could be shown that before the phase transformation, a phase mixture of a monoclinic β-UO_3 phase with a high amorphous proportion is formed which is transformed to orthorhombic U_3O_8 after the phase transition. No indications of segregated Th-rich phases could be detected. This suggests that the Th is somehow incorporated into the structure both before and after the phase transition to U_3O_8.

ACKNOWLEDGEMENTS

This work was carried out as an account of work sponsored by the Government of the Federal Republic of Germany within the Joint Programme on the Technical Development and Further Improvement of IAEA Safeguards between the Federal Republic of Germany and the IAEA. The work was funded by the Federal Ministry for the Environment, Nature Conservation, Nuclear Safety and Consumer Protection, Germany under Task C45/A1961.

REFERENCES

1. S. Boulyga, S. Konegger-Kappel, S. Richter, L. Sangély, *J. Anal. At. Spectrom.* **30**, 1469-1489 (2015).

2. R. Middendorp, M. Klinkenberg, M. Dürr, *J. Radioanal. Nucl. Chem.* **318**, 907-914 (2018).

3. S. Neumeier, R. Middendorp, A. Knott, M. Dürr, M. Klinkenberg, F. Pointurier, D. F. Sanchez, V.-A. Samson, D. Grolimund, I. Niemeyer, D. Bosbach, *MRS Adv.* **3**, 1005-1012 (2018).

4. R. Middendorp, M. Durr, A. Knott, F. Pointurier, D. Ferreira Sanchez, V. Samson, D. Grolimund, *Anal. Chem.* **89**, 4721-4728 (2017).

5. J. Truyens, M. Dürr, Z. Macsik, R. Middendorp, S. Neumeier, S. Richter, G. Stadelmann, C. Venchiarutti, Y. Aregbe. *IRMM-2329P*, 2020: Publications Office of the European Union, Luxembourg.

6. J. Truyens, S. Neumeier, P. Kegler, M. Klinkenberg, M. Zoriy, S. Richter, Y. Aregbe. *Preparation and Certification of the Uranium Oxide Micro Particle Reference Material IRMM-2331P*, 2021: Publications Office of the European Union, Luxembourg.

7. K. G. W. Inn, C. M. Johnson, W. Oldham, S. Jerome, L. Tandon, T. Schaaff, R. Jones, D. Mackney, P. MacKill, B. Palmer, D. Smith, S. LaMont, J. Griggs, *J. Radioanal. Nucl. Chem.* **296**, 5-22 (2012).

8. P. Kegler, F. Pointurier, J. Rothe, K. Dardenne, T. Vitova, A. Beck, S. Hammerich, S. Potts, A.-L. Faure, M. Klinkenberg, *MRS Adv.*, 1-6 (2021).

9. S. K. Potts, P. Kegler, G. Modolo, S. Hammerich, I. Niemeyer, D. Bosbach, S. Neumeier, *MRS Adv.* **7**, 128-133 (2022).

10. S. K. Potts, P. Kegler, G. Modolo, M. Klinkenberg, S. Hammerich, I. Niemeyer, D. Bosbach, S. Neumeier, *MRS Adv.*, (2023).

11. P. Kegler, M. Klinkenberg, A. Bukaemskiy, G. L. Murphy, G. Deissmann, F. Brandt, D. Bosbach, *Materials*. **14**, 6160 (2021).

12. B. H. Toby, *J. Appl. Crystallogr.* **34**, 210-213 (2001).

13. C. Schreinemachers, G. Leinders, G. Modolo, M. Verwerft, K. Binnemans, T. Cardinaels, *Nucl. Eng. Technol.* **52**, 1013-1021 (2020).

14. S. O. Odoh, J. Shamblin, C. A. Colla, S. Hickam, H. L. Lobeck, R. A. Lopez, T. Olds, J. E. Szymanowski, G. E. Sigmon, J. Neuefeind, W. H. Casey, M. Lang, L. Gagliardi, P. C. Burns, *Inorg. Chem.* **55**, 3541-6 (2016).

15. A. E. Shields, A. J. Miskowiec, J. L. Niedziela, M. C. Kirkegaard, K. Maheshwari, M. W. Ambrogio, R. J. Kapsimalis, B. B. Anderson, *Opt. Mater.* **89**, 295-298 (2019).

16. X. Guo, S. V. Ushakov, S. Labs, H. Curtius, D. Bosbach, A. Navrotsky, *Proc. Natl. Acad. Sci. U.S.A.* **111**, 17737-42 (2014).

17. L. Desfougeres, E. Welcomme, M. Ollivier, P. M. Martin, J. Hennuyer, M. Hunault, R. Podor, N. Clavier, L. Favergeon, *Inorg. Chem.* **59**, 8589-8602 (2020).

18. P. Debets, *Acta Cryst.* **21**, 589-593 (1966).

19. T. L. Spano, A. E. Shields, B. S. Barth, J. D. Gruidl, J. L. Niedziela, R. J. Kapsimalis, A. Miskowiec, *Inorg. Chem.* **59**, 11481-11492 (2020).

20. M. Shundalau, A. Zajogin, A. Komiak, A. Sokolsky, D. Umreiko, *J. Spectrosc. Dyn.* **2**, 19 (2012).

21. L. E. Sweet, T. A. Blake, C. H. Henager, S. Hu, T. J. Johnson, D. E. Meier, S. M. Peper, J. M. Schwantes, *J. Radioanal. Nucl. Chem.* **296**, 105-110 (2012).

22. N. B. A. Thompson, V. L. Frankland, J. W. G. Bright, D. Read, M. R. Gilbert, M. C. Stennett, N. C. Hyatt, *J. Radioanal. Nucl. Chem.* **327**, 1335-1347 (2021).

23. R. Rao, R. Bhagat, N. P. Salke, A. Kumar, *Appl. Spectrosc.* **68**, 44-48 (2014).

24. V. K. Tripathi, R. Nagarajan, *Inorg. Chem.* **55**, 12798-12806 (2016).

25. R. Ackermann, A. Chang, C. A. Sorrell, *J. Inorg. Nucl. Chem.* **39**, 75-85 (1977).

26. R. D. Shannon, *Acta Crystallogr. A*. **32**, 751-767 (1976).

27. P. Asplanato, W. Zannouh, A. L. Fauré, P. H. Imbert, J. Lautru, M. Cornaton, N. Dacheux, F. Pointurier, N. Clavier, *J. Nucl. Mater.* **573**, 154142 (2023).

28. R. Paul, C. Keller, *J. Nucl. Mater.* **41**, 133-142 (1971).

29. L. Desgranges, G. Baldinozzi, P. Simon, G. Guimbretière, A. Canizares, *J. Raman Spectrosc.* **43**, 455-458 (2012).

30. M. Razdan, D. W. Shoesmith, *J. Electrochem. Soc.* **161**, H105-H113 (2013).

31. G. Guimbretière, L. Desgranges, A. Canizarès, G. Carlot, R. Caraballo, C. Jégou, F. Duval, N. Raimboux, M. R. Ammar, P. Simon, *Appl. Phys. Lett.* **100**, (2012).

32. H. Idriss, *Surf. Sci. Rep.* **65**, 67-109 (2010).

33. D. Ho Mer Lin, D. Manara, P. Lindqvist-Reis, T. Fanghänel, K. Mayer, *Vib. Spectrosc.* **73**, 102-110 (2014).

34. G. C. Allen, I. S. Butler, T. Nguyen Anh, *J. Nucl. Mater.* **144**, 17-19 (1987).

35. S. D. Senanayake, R. Rousseau, D. Colegrave, H. Idriss, *J. Nucl. Mater.* **342**, 179-187 (2005).

36. E. A. Stefaniak, A. Alsecz, I. E. Sajó, A. Worobiec, Z. Máthé, S. Török, R. V. Grieken, *J. Nucl. Mater.* **381**, 278-283 (2008).

37. C. Jégou, R. Caraballo, S. Peuget, D. Roudil, L. Desgranges, M. Magnin, *J. Nucl. Mater.* **405**, 235-243 (2010).

38. F. Pointurier, O. Marie, *Spectrochim. Acta B*. **65**, 797-804 (2010).

39. A. Miskowiec, J. L. Niedziela, T. L. Spano, M. W. Ambrogio, S. Finkeldei, R. Hunt, A. E. Shields, *J. Nucl. Mater.* **527**, 151790 (2019).

40. L. J. Bonales, J. M. Elorrieta, Á. Lobato, J. Cobos, *Raman spectroscopy, a useful tool to study nuclear materials*. Applications of Molecular Spectroscopy to Current Research in the Chemical and Biological Sciences. (2016).

41. J. M. Elorrieta, L. J. Bonales, N. Rodriguez-Villagra, V. G. Baonza, J. Cobos, *Phys. Chem. Chem. Phys.* **18**, 28209-28216 (2016).

42. M. L. Palacios, S. H. Taylor, *Appl. Spectrosc.* **54**, 1372-1378 (2000).

43. I. S. Butler, G. C. Allen, N. A. Tuan, *Appl. Spectrosc.* **42**, 901-902 (1988).

44. D. Manara, B. Renker, *J. Nucl. Mater.* **321**, 233-237 (2003).

45. E. Enriquez, G. Wang, Y. Sharma, I. Sarpkaya, Q. Wang, D. Chen, N. Winner, X. Guo, J. Dunwoody, J. White, A. Nelson, H. Xu, P. Dowden, E. Batista, H. Htoon, P. Yang, Q. Jia, A. Chen, *ACS Appl. Mater. Interfaces*. **12**, 35232-35241 (2020).